Clustering Predicted by an Electrophysiological Model of the Suprachiasmatic Nucleus

Casey O. Diekman and Daniel B. Forger

J Biol Rhythms 2009 24: 322

DOI: 10.1177/0748730409337601

Clustering Predicted by an Electrophysiological Model of the Suprachiasmatic Nucleus

Casey O. Diekman[*,‡] and Daniel B. Forger[†,‡1]

[*]*Department of Industrial and Operations Engineering,* [†]*Department of Mathematics, and* [‡]*Center for Computational Medicine and Bioinformatics, University of Michigan, Ann Arbor, Michigan*

Abstract Despite the wealth of experimental data on the electrophysiology of individual neurons in the suprachiasmatic nuclei (SCN), the neural code of the SCN remains largely unknown. To predict the electrical activity of the SCN, the authors simulated networks of 10,000 GABAergic SCN neurons using a detailed model of the ionic currents within SCN neurons. Their goal was to understand how neuronal firing, which occurs on a time scale faster than a second, can encode a set phase of the circadian (24-h) cycle. The authors studied the effects of key network properties including: 1) the synaptic density within the SCN, 2) the magnitude of postsynaptic currents, 3) the heterogeneity of circadian phase in the neuronal population, 4) the degree of synaptic noise, and 5) the balance between excitation and inhibition. Their main result was that under a wide variety of conditions, the SCN network spontaneously organized into (typically 3) groups of synchronously firing neurons. They showed that this type of clustering can lead to the silencing of neurons whose intracellular clocks are out of circadian phase with the rest of the population. Their results provide clues to how the SCN may generate a coherent electrical output signal at the tissue level to time rhythms throughout the body.

Key words circadian rhythms, neuronal firing, suprachiasmatic nucleus, mathematical modeling, clustering

Circadian (~24-h) clocks within cells time many biological processes in a broad range of organisms. In mammals, timing is coordinated by the bilateral suprachiasmatic nuclei (SCN) of the hypothalamus. This neuronal network processes signals from the body and the external world, coordinates intracellular rhythms throughout the SCN, and sends signals to the rest of the body to time rhythms in other tissues. While the majority of recent circadian research has focused on the intracellular events that generate timekeeping, there is a growing interest in the network behavior of the SCN (Herzog, 2007; Liu et al., 2007; Freeman et al., 2008). This network operates on multiple scales, as each unilateral SCN contains approximately 10,000 heterogeneous neurons that control rhythms on the time scale of 24 h by the generation of action potentials on time scales quicker than a second.

Because of the complexity of the SCN, many researchers have turned to mathematical modeling to help understand its behavior. Several mathematical models exist for the intracellular generation of circadian rhythms (e.g., Leloup and Goldbeter, 2003; Forger and Peskin, 2003, 2005; Forger et al., 2007) and for the behavior of the overall circadian system (e.g.,

1. To whom all correspondence should be addressed: Daniel Forger, Department of Mathematics, 2074 East Hall, 530 Church Street, University of Michigan, Ann Arbor, MI 48109-1043; e-mail: forger@umich.edu.

JOURNAL OF BIOLOGICAL RHYTHMS, Vol. 24 No. 4, August 2009 322-333
DOI: 10.1177/0748730409337601

Daan and Berde, 1978; Kronauer et al., 1999; Forger et al., 1999). Recent modeling work has focused on the synchronization of cellular clocks within the SCN on a 24-h time scale (Indic et al., 2007, 2008; To et al., 2007; Bernard et al., 2007; Gonze et al., 2005; Bush and Siegelman, 2006) and is part of a growing field studying coupled oscillators (Strogatz, 2000). However, none of these aforementioned studies explicitly model the generation of action potentials by SCN neurons.

Mathematical modeling has also become an established tool for understanding the firing behavior of neurons, beginning with the publication of the Hodgkin-Huxley model of action potential generation in the squid giant axon (Hodgkin and Huxley, 1952). Despite the wealth of experimental data on the electrical activity of SCN neurons, and the well-established modeling techniques in the field of computational neuroscience, modeling the electrical activity of the SCN is relatively new. A Hodgkin-Huxley-type model for the electrical behavior of a single SCN neuron has recently been developed (Sim and Forger, 2007). Here, we use this model to generate the first detailed mathematical model of the electrical activity of the SCN at the tissue level.

The electrical activity of the model SCN could be studied on multiple time scales. One could focus on the 24-h time scale and coarse changes in the frequency of neuronal firing. On this slow time scale, the model would be similar to previous studies (Rohling et al., 2006a, 2006b; Brown and Piggins, 2009). Instead, we focus on the electrical activity over a shorter time scale (up to 1 min), where the circadian clock within individual neurons can be thought of as occupying a set circadian phase. Thus, we are interested in the specific neuronal signals that encode a set circadian phase, analogous to the position of hands on a clock. Even the dynamics of neuropeptides such as vasoactive intestinal peptide (VIP), which can synchronize 24-h rhythms (Aton et al., 2005), are likely slow on this fast time scale (Pakhotin et al., 2006). On this fast time scale, our model can predict the activity of every neuron within the network. We will study the patterns that emerge, including synchronous or asynchronous firing of action potentials across the network. Since we will discuss both the phase of circadian rhythms (time scale of hours) and the phase of neuronal firing (time scale of seconds), we will use the term "circadian phase" to refer to the former and the term "neuronal phase" to refer to the latter to delineate these 2 cases.

Several neurotransmitters have been proposed as candidate synchronizing factors within the SCN, such as VIP, gastrin-releasing peptide (GRP), and γ-aminobutyric acid (GABA). Of these, only GABA is synthesized by most, if not all, SCN neurons (Aton and Herzog, 2005). GABA receptors are also found all throughout the SCN, and while GABA is known to mediate predominantly inhibitory postsynaptic currents there is also evidence that GABA can be excitatory in the SCN (Choi et al., 2008). In this study we use a mathematical model of the electrophysiology of SCN neurons in a network with fast $GABA_A$ inhibition and excitation to predict the electrical activity of the SCN. Since current experimental techniques can only record from a small percentage of SCN neurons, this model gives the first glimpse of the electrical activity of all SCN neurons simultaneously.

MATERIALS AND METHODS

Network Model

We simulated the electrophysiology of the SCN using networks of N = 10,000 interconnected SCN neurons. The dynamics of each neuron i, $i = 1 \ldots N$, was modeled using the Hodgkin-Huxley formalism including sodium, potassium, calcium, background, and synaptic currents as in Sim and Forger (2007). The model equations for the i^{th} neuron were:

$$C\frac{dV_i}{dt} = g_{Na}m_i^3h_i(E_{Na}-V_i) + g_K n_i^4(E_K - V_i) + g_{Ca}r_i f_i(E_{Cai}-V_i) + g_L(E_L - V_i) + I_{syn_i}(t)$$

$$\frac{dq_i}{dt} = \frac{q_{i,\infty} - q_i}{\tau_{q_i}} \qquad q_i = m_i, h_i, n_i, r_i, f_i.$$

The model parameters were taken from the literature or fit to experimental data on individual ionic currents within SCN neurons (see Sim and Forger, 2007, for a complete description of the model formulation). All parameter values used in this study were identical to Sim and Forger (2007), except for the equilibrium values of the sodium gating variables m_∞ and h_∞, which were given slightly modified forms based on reevaluation of experimental data (data not shown):

$$m_{i,\infty} = \frac{1}{1 + \exp(-(V_i + 35.2)/8.1)}$$

$$h_{i,\infty} = \frac{1}{1 + \exp((V_i + 62)/4)}.$$

However, we note that all of the behaviors reported in this study can be obtained using the m_∞ and h_∞ functions that originally appeared in Sim and Forger (2007) as well (data not shown).

To model inhibitory $GABA_A$ coupling in the SCN, we induce an inhibitory current in all neurons that are postsynaptic to a neuron that just fired. We based the form of this inhibitory postsynaptic current (IPSC) on experimental measurements of spontaneous inhibitory postsynaptic potentials (IPSPs) recorded in SCN neurons (Kim and Dudek, 1992). On average, the spontaneous IPSPs reported in Kim and Dudek (1992) had a rise-to-peak time of 7.2 msec and a decay time constant of 14 msec. To produce IPSPs with a similar shape in our model, we use IPSCs that decay exponentially with a time constant of 2 msec. Since the rise time of IPSPs is fast compared with their decay, we assume the rise is instantaneous to gain computational efficiency. The coupling among SCN neurons is implemented through the synaptic current $I_{syn}(t)$:

$$I_{syn_i}(t) = -g_{syn} \sum_{j=1}^{N} \sum_{k} c_{ij} \exp(-(t - t_{j,k})/2).$$

The coupling strength is set by the parameter g_{syn} (higher g_{syn} values result in larger amplitude postsynaptic currents). The binary matrix c keeps track of which neurons are connected ($c_{ij} = 1$ if neuron j is presynaptic to neuron i and 0 otherwise, $j = 1 \ldots N$), and $t_{j,k}$ is the time of the k^{th} spike from cell j. By specifying the connectivity matrix in different ways we simulated different types of connectivity in the SCN. For example, to simulate all-to-all coupling (every SCN neuron connected to every other SCN neuron), we set $c_{ij} = 1$ for all i,j. For sparse connectivity, for each neuron we randomly choose a subset of the N neurons as presynaptic to that neuron (e.g., to simulate 10,000 neurons with 10% connectivity, for each i we set $c_{ij} = 1$ for 1000 randomly chosen j values). To simulate an uncoupled network, we set $c_{ij} = 0$ for all i,j (or alternatively we set $g_{syn} = 0$). To model excitatory $GABA_A$ coupling in the SCN, we simply reverse the sign of all synaptic currents entering a subset of the neurons. All simulations and analysis were conducted using C and MATLAB R2008a (The Mathworks Inc., Natick, MA). The equations were solved using a 5th-order Runge-Kutta method with adaptive stepsize control (Press et al., 1992) and a maximum time step of 1 msec.

Neuronal Heterogeneity

Dissociated SCN neurons grown in low-density cultures maintain circadian rhythms in their electrical activity, but the circadian phase is not synchronized across neurons (Welsh et al., 1995). Thus at any given point of time, the state of the intracellular clock within each neuron is not identical throughout the population. Moreover, since the concentration of intracellular calcium, $[Ca^{2+}]_{in}$, is under the control of the clock (Ikeda et al., 2003), we would expect there to be variation in the levels of $[Ca^{2+}]_{in}$ across a population of isolated neurons as a function of the circadian phase of their intracellular clocks. Since $[Ca^{2+}]_{in}$ is related to the model parameter E_{Ca} (the equilibrium potential for calcium) through the Nernst equation, we simulate this heterogeneity by assigning different values of E_{Ca} to the neurons in our network. We take each neuron's $E_{Ca,i}$ from a normal distribution with a mean of 61 mV and a standard deviation of σ_{Eca}. This gives each neuron a slightly different intrinsic firing frequency. To simulate identical neurons, we set $\sigma_{Eca} = 0$.

Although the intracellular calcium concentration is not the only factor that contributes to the heterogeneity of SCN cells, we find that varying $[Ca^{2+}]_{in}$ alone is sufficient to create significant changes in the intrinsic firing rate of our model SCN neurons. Alternatively, variations in calcium channel conductance (g_{Ca}) or potassium channel conductance (g_K) could be used to alter firing rates in the model as shown in Sim and Forger (2007).

Noise Mechanisms

Synaptic transmission can be a highly unreliable process, with the probability of neurotransmitter release at an individual synapse in vitro ranging from 0.1 to 0.9 in central neurons (Koch, 1999). We simulate this type of synaptic noise by treating synaptic transmission as a binary event with a probability of success p. Whenever a presynaptic neuron fires a spike, for each postsynaptic neuron we draw a random number q from a (0,1) uniform distribution, and if $q < p$ we induce a postsynaptic current in that neuron. Setting $p = 1$ makes synaptic transmission 100% reliable, while setting $p = 0$ corresponds to uncoupled neurons.

In addition to synaptic transmission being a probabilistic event, there is also randomness in the amplitude of the postsynaptic response. In a study of a rat neocortical pyramidal cell, the variance in the size of evoked postsynaptic potentials was as large as the mean (Koch, 1999). To incorporate this type of variability in our simulations, for each successful synaptic transmission we randomly choose the synaptic conductance for that event to be anywhere in the interval $[g_{syn} \pm k \times g_{syn}/2]$. Setting $k = 0$ corresponds to no randomness in the amplitude of postsynaptic currents. In this study we limit ourselves to $k \leq 2$.

Order Parameters

To quantify the synchrony of a population of spiking neurons, we compute an order parameter R as in (Garcia-Ojalvo et al., 2004; Golomb and Rinzel, 1994). Golomb and Rinzel (1994) defined the order parameter as the ratio of the time-averaged fluctuations of the population-averaged voltage across all N neurons, $V(t) = \frac{1}{N}\sum_{i=1}^{N} V_i(t)$, over the population average of each cell's time-averaged V_i fluctuations:

$$R = \frac{\mathrm{var}(V)}{\frac{1}{N}\sum_{i=1}^{N} \mathrm{var}(V_i)}.$$

If the population is completely disordered, then $R \approx 0$; on the other hand, if the population is fully synchronized, then $R \approx 1$. An intermediate R value indicates partial synchronization.

In addition to R, we also calculate the higher-order parameters, z_n, which detect the segregation of a population of coupled oscillator into n clusters as described in Golomb and Hansel (2000):

$$Z_n = \frac{1}{N}\sum_{i=1}^{N} e^{in\phi_i}$$

where ϕ_i is the neuronal phase of the i^{th} neuron (defined below). For example, if a population forms 3 equally sized clusters oscillating 1/3 out of neuronal phase with each other, then $z_1 = z_2 = 0$ while $z_3 = 1$. We define ϕ_i as:

$$\phi_i(t) = \left(\frac{t - t_{lap}}{t_{nap} - t_{lap}}\right) \times 2\pi$$

where t_{lap} is the time of the last action potential from neuron i before t, and t_{nap} is the time of the next action potential from neuron i after t. Neurons that did not fire were excluded from higher-order parameter analyses.

RESULTS

Here, we describe results from simulations that predict the electrical activity of the SCN. Our simulations contained 10,000 individual SCN neurons which communicated via inhibitory GABA postsynaptic potentials. Inhibitory coupling did not lead to desynchronized firing throughout the SCN, rather we found that large "clusters" of SCN neurons fired synchronously (e.g., see Fig. 1B, C).

We then studied how the clustering depends on network properties such as the synaptic strength and density, as well as the amount of heterogeneity in the neuronal population. Our simulations tracked the electrical behavior of every SCN neuron within a lobe. Since it is only possible to experimentally record from 100 or fewer of the 10,000 SCN neurons, we make testable predictions about the clustering of electrical activity in recordings from a small number of neurons by analyzing the behavior of 100 neurons randomly sampled from the 10,000 neurons in our simulations.

Order and Disorder in the SCN

Simulation of 10,000 uncoupled SCN neurons ($g_{syn} = 0$) with random initial states showed spontaneous, desynchronized firing. In these uncoupled network simulations, we found no evidence of coordinated firing throughout the SCN (see Fig. 1A, B). This disordered state was characterized by an order parameter near zero (R = 1.35E-4 ± 3.39E-5, mean ± SD of 100 simulations for the uncoupled case with different initial conditions). To simulate the effect of fast $GABA_A$ inhibitory postsynaptic potentials, the most prevalent signal among SCN neurons, we modeled inhibitory coupling between SCN neurons. Our initial simulations coupled each neuron to all other neurons (all-to-all coupling). While neurons in these simulations started in random initial states, we found that coordinated behavior emerged within the first few seconds of the simulations. The inhibitory coupling caused the formation of clusters where large fractions of the SCN fired synchronously. Given sufficient time, we found that this clustered firing behavior occurred for all coupling strengths. Figure 1C-F shows this

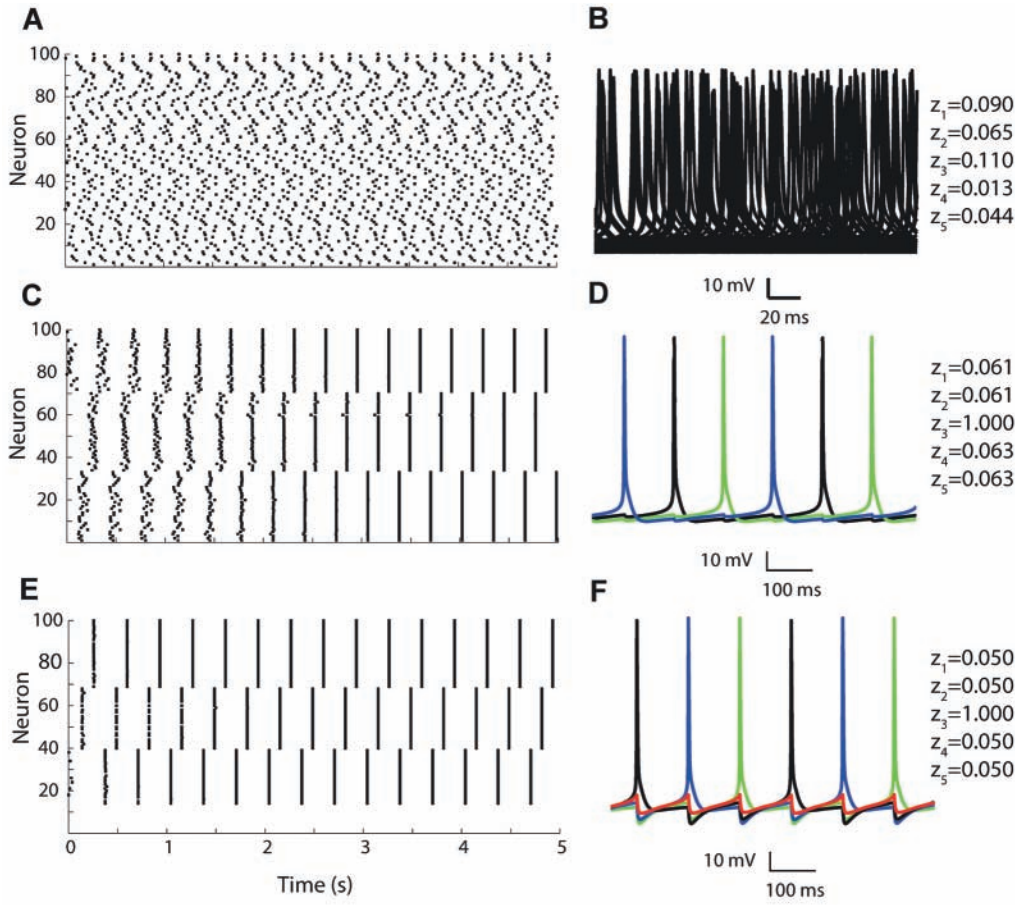

Figure 1. Formation of clusters in simulations of 10,000 homogeneous suprachiasmatic nuclei neurons. (A, B) Uncoupled neurons. (A) Spike raster of 100 randomly chosen neurons demonstrate that without coupling each neuron spikes regularly with its phase dependent only on initial conditions. No patterns in spike timings across the population are evident. (B) Voltage traces of the 100 neurons for the 20th second of simulation. Order parameter $R \approx 0$ **and low values of the higher-order parameters (z_1 through z_5 at t = 19 sec) indicate the voltage trajectories are completely asynchronous. (C, D) Inhibitory all-to-all coupling, g_{syn} = 0.001. Neurons quickly segregate into 3 clusters, within each cluster all neurons spike in synchrony and follow the same voltage trajectory. (D) The blue, black, and green clusters contain 3406, 3364, and 3230 neurons, respectively. The presence of 3 clusters is confirmed by the higher-order parameter z_3 = 1.00 at t = 19 sec. The 3 clusters themselves fire out of phase with each other, resulting in an R value around 0.29. (E, F) Inhibitory all-to-all coupling, g_{syn} = 0.01. Neurons almost immediately segregate into 4 clusters, 3 of which consist of spiking neurons while the neurons in the 4th cluster never spike. (F) The blue, black, green, and red clusters contain 2865, 2844, 2793, and 1498 neurons, respectively. z_3 = 1.00 at t = 19 sec (calculated based on the phases of spiking neurons only) confirms there are 3 clusters of spiking neurons. The presence of the silenced cluster leads to a slightly lower R value (0.27) than the 3-cluster state.**

behavior for 2 coupling strengths. In each case, 3 groups of firing neurons were formed and the time between the firing of each cluster was approximately constant. Here, the order parameter R was approximately 1/3, which indicated partial synchronization and also suggested the presence of 3 synchronously firing groups (R = 0.29 ± 5.91E-4 over 100 simulation replications with g_{syn} = 0.001). We verified the existence of a 3-cluster state visually using the voltage traces and by calculating higher-order parameters z_1 through z_5 (e.g., see Figs. 1 and 2). We consistently found agreement between the clustered state seen visually and the values of R and higher-order parameters. We also noticed that the order parameter decreased slightly for the higher coupling strength (R = 0.27 ± 5.91E-4 over 100 simulation replications with g_{syn} = 0.01). In this case the SCN was divided into 4 clusters, 3 clusters firing out of neuronal phase with the other clusters and a 4th group of neurons that did not fire. These results led us to hypothesize that $GABA_A$ coupling could indeed produce an ordered state of the SCN.

At both coupling strengths, we found that the size of the clusters varied depending on initial conditions. For example, with g_{syn} = 0.001 the size of the largest of the 3 clusters ranged from 3379 to 3459 while the size of the smallest cluster ranged from 3194 to 3286 over the 100 simulation replications. With g_{syn} = 0.01, the number of neurons that were silenced ranged from 1376 to 2178.

Exploring Network Properties of the SCN

Many of the network properties of the SCN, such as the coupling strength and the degree of connectivity, are difficult to measure experimentally. We can explore such properties using our model, and

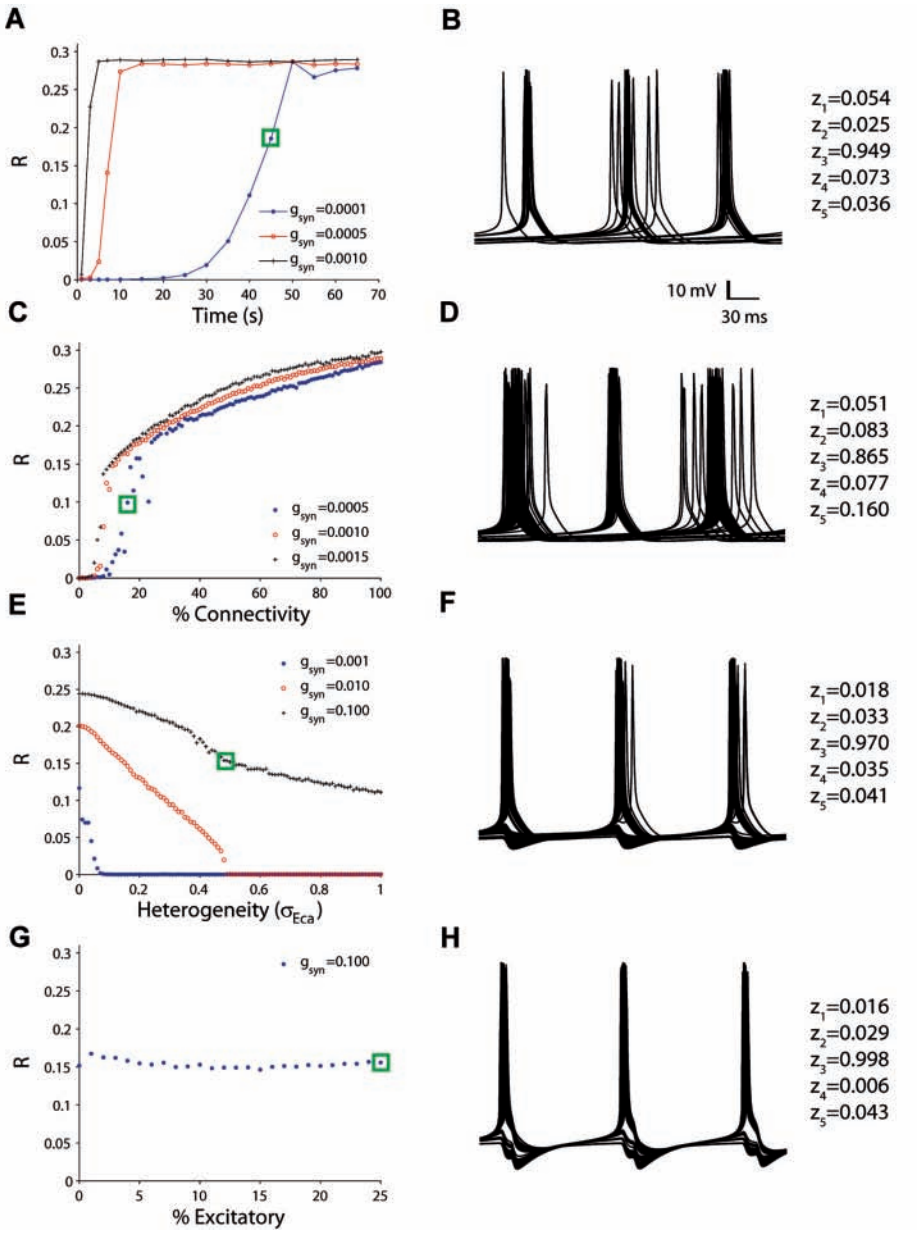

Figure 2. Clustering depends on network properties. (A, C, E, G) Each R value is computed for the 60th second of a 10,000 neuron simulation. In A-D the neuronal population is homogenous. (A) As the coupling strength (g_{syn}) decreases, it takes longer for the 3-cluster state to form ($R \approx 0.3$). Simulations are with all-to-all coupling. (B) Voltage traces of 100 randomly chosen neurons for the 45th second of simulation with $g_{syn} = 0.0001$ and $z_3 = 0.95$ at $t = 44$ seconds indicate that the network is transitioning to the 3-cluster state but that some neurons have not yet joined a cluster. (C) The synaptic density (% connectivity) of the network affects the degree of clustering. With very low connectivity, the network behaves as if the neurons are uncoupled. For each coupling strength (g_{syn}), as the connectivity is increased there appears to be a value at which the network transitions from a disordered state ($R \approx 0$) to one that exhibits some order ($R > 0$). As the connectivity approaches 100% (all-to-all coupling), the network goes to the 3-cluster state ($R \approx 0.3$). At lower connectivities, R values close to 0.3 are occasionally seen for certain initial conditions (data not shown). (D) Voltage traces of 100 neurons randomly chosen from a network with $g_{syn} = 0.0005$ and 16% connectivity show 3 clusters still in the process of forming ($z_3 = 0.87$ at $t = 59$ sec). (E) As the amount of heterogeneity in the intrinsic firing rate and dynamics of the neuronal population (σ_{Eca}) is increased, the degree of order in the network decreases. Simulations are with 10% connectivity. (F) Clustering is still evident in a network with $g_{syn} = 0.1$, 10% connectivity, and $\sigma_{Eca} = 0.5$ ($z_3 = 0.97$ at $t = 59$ sec). (G) As the percentage of neurons in the network that respond to GABA with excitation rather than inhibition is increased from 0 to 25%, little effect is seen on the clustering behavior (R nearly constant). Simulations are with 10% connectivity and $\sigma_{Eca} = 0.5$. (H) The coherence of neurons within each cluster appears to be enhanced by including excitatory effects of GABA in 25% of neurons in the network compared with the all-inhibitory network of panel F ($z_3 = 1.00$ at $t = 59$ sec).

determine if the clustering behavior persists for a wide enough range of parameter values to include those likely present in the SCN. We first lowered the coupling strength (Fig. 2A, B) and found that even at very low coupling strengths (e.g., 100-fold less than those used in Fig. 1E, F) clustering of neuronal states still emerged. The transition from a disordered state to an ordered state was delayed by up to a minute at low coupling values. Figure 2B shows a network that is transitioning to the ordered state and the consolidation of spikes into a cluster. We also explored higher coupling strengths, and found that for $g_{syn} \geq 0.1$ all-to-all coupling produced large hyperpolarizations of the membrane (data not shown).

In the actual SCN, a given neuron only synapses onto a fraction of other SCN neurons. To explore the effect of partial connectivity, we performed a series of simulations with increasing connectivity, beginning with simulations in which each neuron synapses onto just 1% of the network up to simulations with 99%

connectivity. In each simulation the specific synaptic connections were chosen randomly. For each connected SCN, we also simulated a variety of coupling strengths. At the moderate and high coupling strengths, clusters began forming within the first 60 sec of simulation with network connectivity as low as 5% to 10% (Fig. 2C). At low coupling strength and low connectivity, clustering was not observed during the first 60 sec of simulation (Fig. 2C), but clusters did form after a long initial transient (data not shown) similar to the simulations shown in Figure 2A.

Recordings from small populations of SCN neurons show that at a given time of day there is heterogeneity in the firing frequencies of individual neurons (Brown and Piggins, 2007). We simulate heterogeneity in firing frequency through variation in the equilibrium potential for calcium (E_{Ca}) of the neurons. The rationale for this approach is that E_{Ca} is related to the intracellular calcium concentration of SCN neurons, which has been demonstrated to be under the control of the circadian clock (Ikeda et al., 2003). Moreover, a study by Quintero et al. (2003) suggests a correlation between the firing frequency of a SCN neuron and the state of its intracellular clock (Brown and Piggins, 2007). By allowing different values of E_{Ca} for the neurons in our simulation, each neuron has slightly different dynamics and firing frequency corresponding to the circadian phase of its intracellular clock. When these heterogeneous SCN neurons were simulated, we found that clustering could still occur. However, larger amounts of heterogeneity required larger coupling strengths for clustering (Fig. 2E). The firing within clusters from the heterogeneous network was not perfectly synchronized, referred to as "smeared clusters" (Golomb and Hansel, 2000), and not all neurons were firing as part of a cluster during the 60th second of simulation (Fig. 2F). This explains why the order parameters for these simulations were below 1/3.

While the majority of GABA transmissions between SCN neurons are inhibitory, excitatory effects of GABA have been reported in a minority (less than 25%) of SCN neurons (Choi et al., 2008). To test whether such excitatory responses affect the behavior of our network simulations, we had GABA induce EPSPs rather than IPSPs in a subset of the neurons in our network. Even if 25% of the neurons responded to GABA with excitation, the network simulations and clustering behavior were relatively unaffected. However, if the majority of connections were excitatory, the network could organize into a state in which all neurons fire synchronously in 1 cluster (data not shown). Interestingly, having an excitatory effect of GABA on a minority of neurons in the network seems to lead to increased coherence within the clusters compared with an all-inhibitory network (compare Fig. 2F and H) suggesting a possible functional role for excitatory GABA in the SCN.

Dynamic Clustering in the SCN

A morphometric study by Guldner (1984) estimated an average of 11,900 neurons and 1,264 synaptic appositions per neuron in the SCN of female rats. Based on this experimental estimate, we, from now on, examine closely the results of simulations with 10% connectivity to predict the firing behavior of the SCN. In simulations with 10% connectivity and heterogeneity (σ_{Eca} = 0.5), we detected the presence of clusters with near synchronous firing by calculating the instantaneous firing rate of the population (the total number of spikes being fired across the SCN in each millisecond) as shown in Figure 3A and B. Without coupling (g_{syn} = 0), there was a relatively constant low level of firing across the network throughout time (Fig. 3A). With coupling (g_{syn} = 0.1), there were extended periods of inactivity with very little firing across the network punctuated by bursts of 500 or more neurons firing synchronously (Fig. 3B). Each time a cluster fired, the total number of neurons firing together was not necessarily the same as in the previous firing of that cluster (Fig. 3B). This behavior can be understood via the raster plot in Figure 3C, showing spiking from 100 neurons randomly chosen from the network. The neurons are sorted vertically according to their earliest spike time (after the 15th second) to make the 3 clusters clearly visible. The membership of the clusters was not constant but rather changed over time, referred to as "dynamic clustering" (Terman et al., 2008). A few examples of individual neurons that do not reliably fire within the same cluster throughout the 5 sec of simulation are shown in Figure 3C: 1) neuron 57 originally fired with the middle cluster, but after 2 cycles it switched and joined the bottom cluster; 2) neuron 78 initially fired with the top cluster, but did not fire in the last several cycles; and 3) neuron 25 was silent for the first 14 cycles, but then fired with the bottom cluster in the last 2 cycles.

Output Signal of the SCN

The clustering of SCN neurons has a major effect on the firing rate of individual neurons, which is the main output signal of the SCN. When uncoupled,

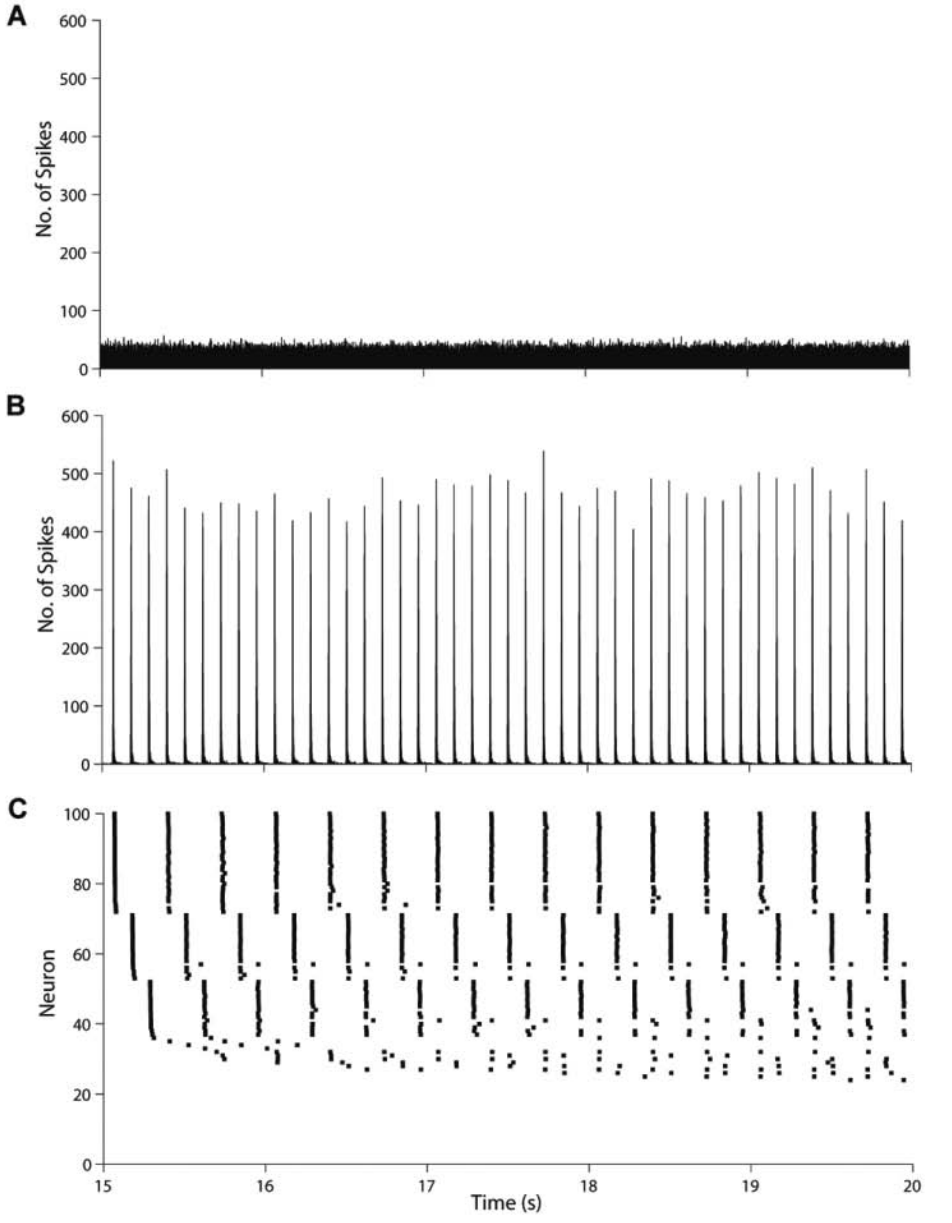

Figure 3. Dynamic clustering in a 10,000-neuron network with sparse coupling and heterogeneity. (A) **Uncoupled neurons with heterogeneity. The instantaneous firing rate of the population, calculated as the number of action potentials per millisecond, randomly fluctuates around a mean value of 50 throughout the simulation. (B) Sparse coupling (10% connectivity, g_{syn} = 0.1) with heterogeneity (σ_{Ecal} = 0.5). The instantaneous firing rate of the population is near zero for most of the time bins, punctuated by bursts of activity where up to 500 neurons fire in the same millisecond time bin. (C) The spike raster of 100 randomly chosen neurons reveals that these bursts of spiking activity correspond to 3 clusters of neurons. However, unlike the clusters in homogeneous networks with all-to-all coupling, the size and membership of the clusters in heterogenous networks with sparse coupling are not constant over time. The neurons are sorted vertically so that during the 15th second of simulation the neurons that spike together in a cluster are plotted contiguously. Neuron 57 is initially in the middle cluster but by the 16th second of simulation has joined the bottom cluster. Neuron 78 initially fires with the top cluster 4 of 5 cycles but then does not fire during the next 3 sec of simulation. Neurons 1 through 24 do not fire at all during these 5 sec of simulation.**

simulated heterogeneous neurons fired regularly between 3 and 3.9 Hz (firing rates approximately normally distributed, 3.45 ± 0.11 Hz). When coupled, the majority of neurons (~6000) fired at around 3 Hz, but a substantial portion (~2000 neurons) was silenced. The remaining neurons fired at rates anywhere between 0 and 3 Hz. By comparing an individual neuron's firing rate when uncoupled to its firing rate in the coupled network, we see that neurons with lower intrinsic firing rates are silenced (compare Fig. 4A and C). Also, neurons that have higher intrinsic firing rates are slowed down to 3 Hz (compare Fig. 4B and D). Thus, the coupling and the resulting clustering of SCN neurons allows the majority of heterogeneous SCN neurons to agree on a single firing rate (interquartile range of firing rates was 0.1 Hz for neurons in Fig. 4B and 0 Hz for neurons in Fig. 4D), while most neurons that are too slow to keep up with this rate are silenced. Presumably this coordination of firing rates strengthens the output signal of the SCN to more reliably time rhythms throughout the body.

We also computed interspike interval (ISI) histograms (Fig. 4E, F) for individual neurons in a coupled simulation to compare to previously published experimental data on SCN

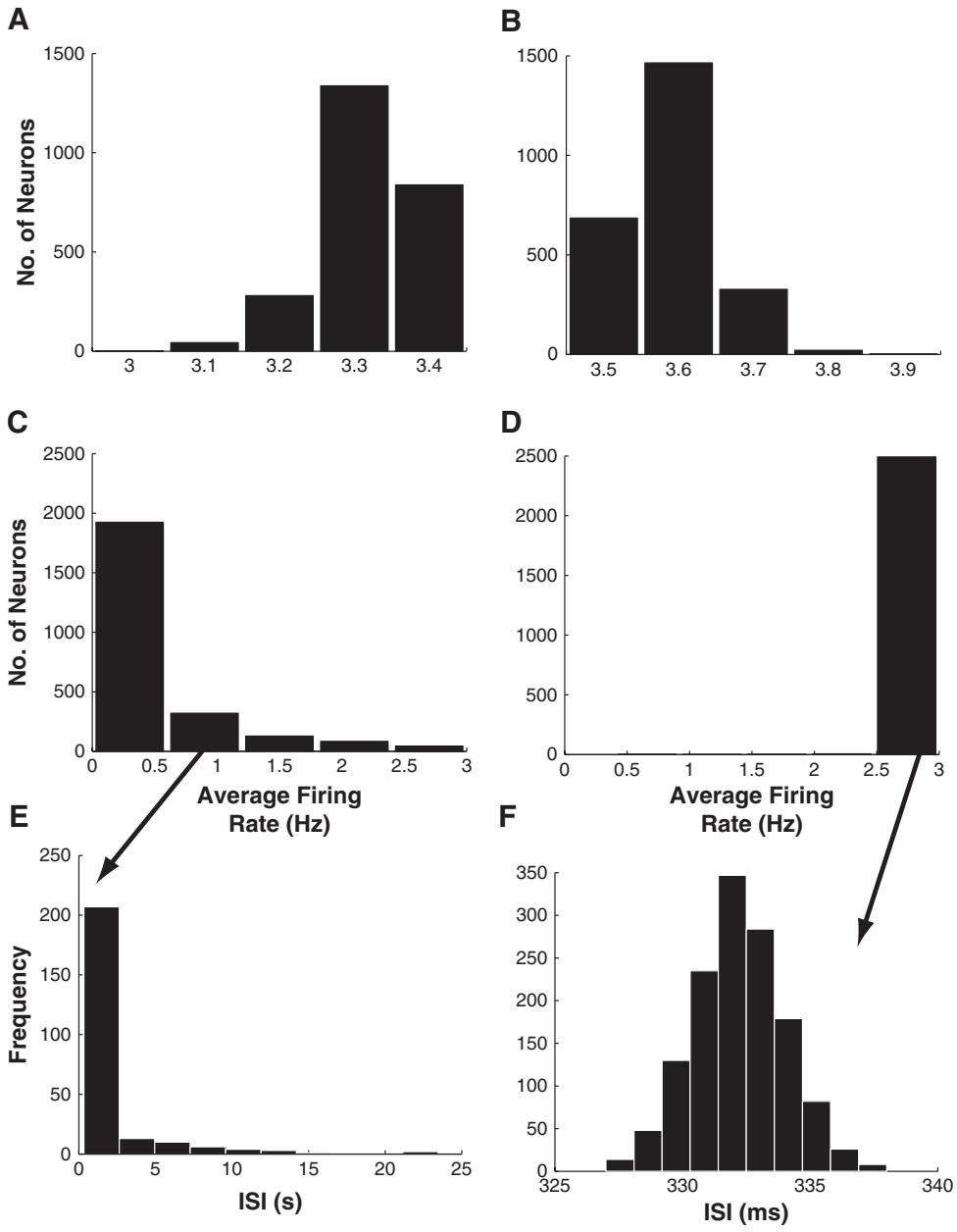

Figure 4. Effect of dynamic clustering on the output signal of the suprachiasmatic nuclei (SCN). (A, B) A total of 10,000 uncoupled neurons (same simulation as Fig. 3A). The firing rates of individual neurons (averaged over the last 10 sec of simulation) are normally distributed due to heterogeneity in the equilibrium potential for calcium (E_{Ca}) across the network. (A) Histogram of the firing rates for the 2500 neurons with the slowest intrinsic firing rate ($E_{Ca} \leq 60.66$ mV). (B) Histogram of the firing rates for the 2500 neurons with the fastest intrinsic firing rate ($E_{Ca} \geq 61.33$ mV). (C, D) Sparse coupling (10% connectivity, g_{syn} = 0.1) with heterogeneity (σ_{Eca} = 0.5) (same simulation as Fig. 3B). Around 6000 neurons fire regularly with a cluster at around 3 Hz, but almost 2000 are silenced. The remaining neurons have intermediate firing rates due to switching between clusters or being silenced transiently. The neurons that have slower intrinsic firing rates (due to the state of their intracellular clock) tend to be silenced by the network, while neurons with medium to higher intrinsic firing rates (again due to the state of their intracellular clock) are slowed down to agree on a firing rate of 3 Hz. (C) Histogram of the firing rates for the 2500 neurons with the slowest intrinsic firing rate ($E_{Ca} \leq 60.66$ mV). (D) Histogram of the firing rates for the 2500 neurons with the fastest intrinsic firing rate ($E_{Ca} \geq 61.35$ mV). (E) Interspike interval (ISI) histogram for an individual neuron with an average firing rate of 0.5 Hz. The ISI distribution is skewed to the right, matching experimental data from irregularly firing SCN neurons (Kononenko and Dudek, 2004). (F) ISI histogram for an individual neuron with an average firing rate of 3 Hz. The ISI distribution is approximately normal, matching experimental data from regularly firing SCN neurons (Kononenko and Dudek, 2004).

firing. In Kononenko and Dudek (2004), recordings from neurons in slices of rat SCN revealed 2 distinct firing behaviors for SCN neurons. Some of the neurons they recorded from exhibited "regular" firing, characterized by an approximately normal ISI distribution, while other SCN neurons exhibited slower "irregular" firing, characterized by a skewed ISI distribution with a long right tail. We find both of these behaviors in our network simulations: a neuron firing regularly at ~3 Hz shows an approximately normal ISI distribution (Fig. 4F), while a neuron firing irregularly at ~0.5 Hz exhibits a skewed ISI distribution (Fig. 4E).

Clustering in the Presence of Synaptic Noise

Synaptic transmission is stochastic and not 100% reliable (Koch, 1999). To investigate the effect of this stochasticity on the coupled network, we simulated synaptic noise by varying the probability with which presynaptic spikes resulted in a postsynaptic current (Fig. 5A). We also incorporated variation in the magnitude of the postsynaptic currents in response to a presynaptic spike (Fig. 5B). Even when both of these sources of noise are present, the instantaneous firing rate of the population indicates that clustering still persists (Fig. 5C). Since we find clustering in a noisy network of

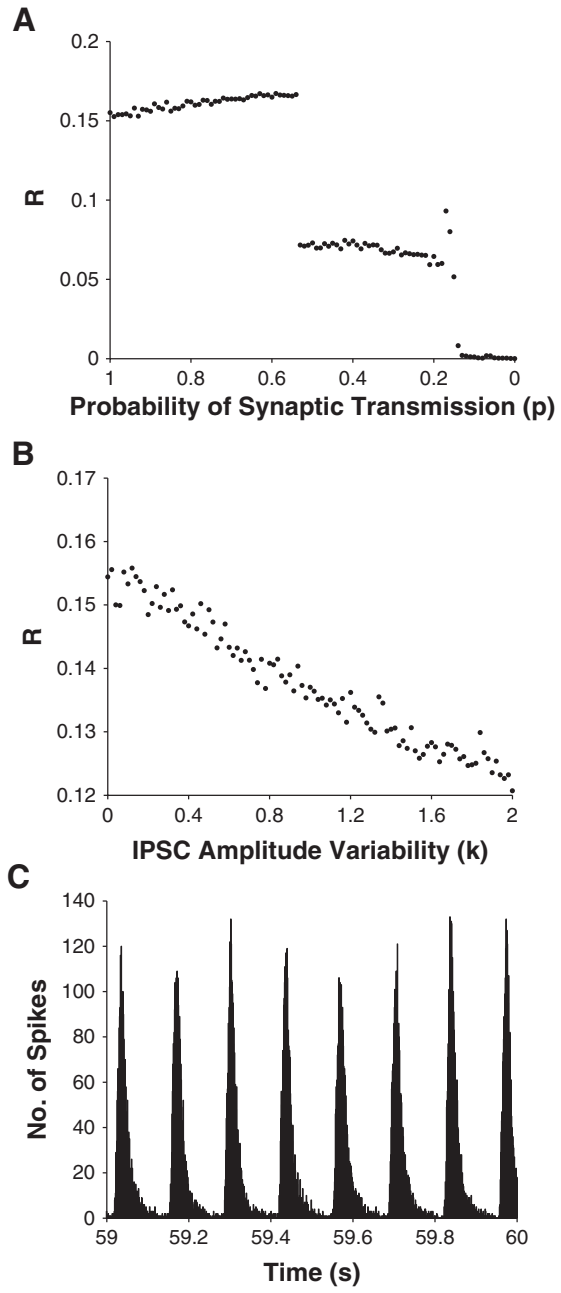

Figure 5. Clustering persists in the presence of synaptic noise. (A) The probability of a successful synaptic transmission is lowered from 100% reliable (p = 1) to no transmission (p = 0). Clustering is unaffected in simulations with g_{syn} = 0.1, 10% connectivity, and σ_{Eca} = 0.5 up to approximately p = 0.5. For p = 0.2-0.5, the network switches to a more disordered state, although 3 smeared clusters are still present. For p < 0.2, no clustering is detected. (B) Variability in the amplitude of inhibitory postsynaptic currents (IPSCs) is increased from no variability (k = 0) to the maximum variability possible while still ensuring all PSCs are inhibitory (k = 2) with g_{syn} = 0.1 (see Materials and Methods section for details). Clustering persists throughout this range (simulations are with 10% connectivity, σ_{Eca} = 0.5, and p = 1). (C) Simulation with both types of synaptic noise (g_{syn} = 0.1, 10% connectivity, σ_{Eca} = 0.5, p = 0.5, and k = 1). The instantaneous firing rate of the population, calculated as the number of action potentials per millisecond, indicates clustering persists despite this noise.

sparsely connected heterogeneous SCN neurons, we predict that clustering may indeed be occurring in the SCN in vivo.

DISCUSSION

Based on simulations of the SCN as an inhibitory network, we predict that the SCN forms clusters in which neurons fire in near synchrony. Furthermore, we predict that the membership of these clusters may change over time. While these are novel predictions with respect to the SCN, clustering has been reported before in a number of other models of inhibitorily coupled oscillators. Several studies report clustering in globally coupled phase-only oscillators (e.g., Golomb et al., 1992; Okuda, 1993). Golomb and Rinzel (1994) observe clustering in a model of globally coupled reticular thalamic neurons, and note that adding noise to the neuronal dynamics can cause neurons to hop from cluster to cluster. Golomb and Hansel (2000) observe smeared clusters in either heterogeneous or sparse networks of integrate-and-fire neurons. Terman et al. (2008) studied dynamic clustering in sparsely connected excitatory-inhibitory networks. In our study we have tried to include many features of the physiology and complexity of the SCN by studying a predominantly inhibitory network with heterogeneity, sparse connectivity, and synaptic noise. Future work could include modeling electrotonic coupling and synaptic delays. To our knowledge this study is the first to suggest clustering in the SCN.

While clustering has appeared in many other neuronal models, there are relatively few studies that report having found clustering in experimental recordings. One example is Terman et al. (2008), which hints that dynamic clustering may be present in recordings from neurons within the insect antennal lobe. Without reporting clustering explicitly, there are several other experimental studies that indicate the importance of inhibition in synchronizing neurons in the hippocampus, thalamus, and the locust olfactory system (see discussion section in Tiesinga and Jose, 2000). In Traub et al. (1996), $GABA_A$ receptor-mediated inhibition was shown to be the mechanism behind synchronization in hippocampal slices. Tiesinga and Jose (2000) distinguish weak synchronization, in which the average neuronal activity of the population is periodic without each neuron firing in each period, from strong synchronization, in which each neuron fires within a short interval of each other, and claim that weak synchronization is consistent with the experimental recordings in Traub et al. (1996). While

such synchronization has not yet been reported in experimental studies of the SCN, we predict that such synchronization may indeed be occurring in the SCN, since $GABA_A$ receptor-mediated inhibition leads to clustering (a form of weak synchronization) in our model. Our model also predicts that such clustering will only occur if there is sufficient coupling strength and connectivity to overcome heterogeneity of circadian phase in the network. These conditions may not be met in cultures of dissociated SCN neurons or SCN slices, or admittedly even in vivo. If this is the case, then we would not expect clustering to occur in the SCN. However, if clustering is found in the SCN, the SCN would be a viable experimental system to study properties of clustering.

If clustering does occur in the SCN, what might its role be in terms of rhythm generation? One possibility is that many neurons firing in near synchrony could potentially send a stronger signal to other brain areas than individual neurons firing out of neuronal phase with each other. Additionally, if the firing rate of individual SCN neurons communicates time of day information, then the formation of clusters tends to either silence or adjust the firing rate of neurons whose intracellular clocks are out of circadian phase with the population average. Also, in our simulations, we have found that for the same parameters, different 3-cluster solutions are possible depending on initial conditions. Chandrasekran et al. (2009) points out that such behavior allows a single network of neurons to be able to transmit multiple pieces of information in the form of temporal codes. This ability could be extremely useful for the SCN, given that it is a relatively small brain structure but needs to time many diverse rhythms throughout the body.

We have focused on GABAergic neural coupling in this study since GABA is by far the most prevalent intrinsic neurotransmitter in the SCN. However, we do note that there have been reports of neuronal synchronization in the SCN in the absence of synaptic transmission (Bouskila and Dudek, 1993). Using our modeling framework, many more details of SCN anatomy and physiology could be incorporated. For example, the SCN is commonly believed to have distinct subdivisions, a ventral "core" and a dorsal "shell," with characteristic neuropeptide expression and projections (Moore and Silver, 1998). In our model, we could simulate this by giving a subset of neurons in the network certain properties, for example, by making them VIPergic or possessing the VIP receptor $VPAC_2$, and then control which other subsets of neurons they are connected to in accordance with the known densities of projections. We also plan to integrate this model with existing detailed models of the intracellular clock to help understand the link between the molecular biology and electrophysiology of circadian timekeeping.

ACKNOWLEDGMENTS

DBF is an Air Force Office of Scientific Research Young Investigator (Air Force Grant FA9550-08-1-0076). COD is a Graduate Research Fellow of the National Science Foundation. We would like to thank Mino Belle, Cecilia Diniz Behn, Richard Yamada, and Erik Herzog for important discussions.

REFERENCES

Aton SJ, Colwell CS, Harmar AJ, Waschek J, and Herzog ED (2005) Vasoactive intestinal polypeptide mediates circadian rhythmicity and synchrony in mammalian clock neurons. Nat Neurosci 8:476-473.

Aton SJ and Herzog ED (2005) Come together, right . . . now: Synchronization of rhythms in a mammalian circadian clock. Neuron 48:531-534.

Bernard S, Gonze D, Cajavec B, Herzel H, and Kramer A (2007) Synchronization-induced rhythmicity of circadian oscillators in the suprachiasmatic nucleus. PLoS Comput Biol 3:667-679.

Bouskila Y and Dudek FE (1993) Neuronal synchronization without calcium-dependent synaptic transmission in the hypothalamus. Proc Natl Acad Sci U S A 90: 3207-3210.

Brown TM and Piggins HD (2007) Electrophysiology of the suprachiasmatic circadian clock. Prog Neurobiol 82: 229-255.

Brown TM and Piggins HD (2009) Spatiotemporal heterogeneity in the electrical activity of suprachiasmatic nuclei neurons and their response to photoperiod. J Biol Rhythms 24:44-54.

Bush WS and Siegelman HT (2006) Circadian synchrony in networks of protein rhythm drive neurons. Complexity 12:67-72.

Chandrasekaran L, Matveev V, and Bose A (2009) Multistability of clustered states in a globally inhibitory network. Physica D 238:253-263.

Choi HJ, Lee CJ, Scroeder A, Kim YS, Jung SH, Kim JS, Kim DY, Son EJ, Han HC, Hong SK, et al. (2008) Excitatory actions of GABA in the suprachiasmatic nucleus. J Neurosci 28:5450-5459.

Daan S and Berde C (1978) Two coupled oscillators: Simulations of the circadian pacemaker in mammalian activity rhythms. J Theor Biol 70:297-313.

Forger DB, Gonze D, Virshup D, and Welsh DK (2007) Beyond intuitive modeling: Combining biophysical models with innovative experiments to move the circadian clock field forward. J Biol Rhythms 22:200-210.

Forger DB, Jewett ME, and Kronauer RE (1999) A simpler model of the human circadian pacemaker. J Biol Rhythms 14:532-537.

Forger DB and Peskin CS (2003) A detailed predictive model of the mammalian circadian clock. Proc Natl Acad Sci U S A 100:14806-14811.

Forger DB and Peskin CS (2005) Stochastic simulation of the mammalian circadian clock. Proc Natl Acad Sci U S A 102:321-324.

Freeman GM, Webb AB, Sungwon AN, and Herzog ED (2008) For whom the bells toll: Networked circadian clocks. Sleep Biol Rhythms 6:67-75.

Garcia-Ojalvo J, Elowitz MB, and Strogatz SH (2004) Modeling a synthetic cellular clock: Repressilators coupled by quorum sensing. Proc Natl Acad Sci U S A 101:10955-10960.

Golomb D, Hansel D, Shraiman B, and Sompolinsky H (1992) Clustering in globally coupled phase oscillators. Phys Rev A 45:3516-3530.

Golomb D and Rinzel J (1994) Clustering in globally coupled inhibitory neurons. Physica D 72:259-282.

Golomb D and Hansel D (2000) The number of synaptic inputs and the synchrony of large, sparse neural networks. Neural Comput 12:1095-1139.

Gonze D, Bernard S, Waltermann C, Kramer A, and Herzel H (2005) Spontaneous synchronization of coupled circadian oscillators. Biophys J 89:120-129.

Guldner FH (1984) Suprachiasmatic nucleus: Numbers of synaptic appositions and various types of synapses. Cell Tissue Res 235:449-452.

Herzog ED (2007) Neurons and networks in daily rhythms. Nat Neurosci 8:790:802.

Hodgkin AL and Huxley AF (1952) A quantitative description of membrane current and its application to conduction and excitation in nerve. J Physiol 117:500-544.

Ikeda M, Sugiyama T, Wallace CS, Gompf HS, Yoshioka T, Miyawaki A, and Allen CN (2003) Circadian dynamics of cytosolic and nuclear Ca2+ in single suprachiasmatic nucleus neurons. Neuron 38:253-263.

Indic P, Schwartz WJ, Herzog ED, Foley NC, and Antle MC (2007) Modeling the behavior of coupled cellular circadian oscillators in the suprachiasmatic nucleus. J Biol Rhythms 22:211-219.

Indic P, Schwartz WJ, and Paydarfar D (2008) Design principles for phase-splitting behaviour of coupled cellular oscillators: Clues from hamsters with 'split' circadian rhythms. Journal of the Royal Society Interface 5: 873-883.

Kim YI and Dudek FE (1992) Intracellular electrophysiological study of suprachiasmatic nucleus neurons in rodent: Inhibitory synaptic mechanisms. J Physiol 458: 247-260.

Koch C (1999) *Biophysics of Computation.* New York: Oxford University Press.

Kononenko NI and Dudek FE (2004) Mechanism of irregular firing of suprachiasmatic nucleus neurons in rat hypothalamic slices. J Neurophysiol 91:267-273.

Kronauer RE, Forger DB, and Jewett ME (1999) Quantifying human circadian pacemaker response to brief, extended, and repeated light stimuli over the phototopic range. J Biol Rhythms 14:500-515.

Leloup JC and Goldbeter A (2003) Toward a detailed computational model for the mammalian circadian clock. Proc Natl Acad Sci U S A 100:7051-7056.

Liu AC, Welsh DK, Ko CH, Tran HG, Zhang EE, Priest AA, Buhr ED, Singer O, Meeker K, Verma IM, et al. (2007) Intercellular coupling confers robustness against mutations in the SCN circadian clock network. Cell 129: 605-616.

Moore RY and Silver R (1998) Suprachiasmatic nucleus organization. Chronobiol Int 15:475-487.

Okuda K (1993) Variety and generality of clustering in globally coupled oscillators. Physica D 63:424-436.

Pakhotin P, Harmar AJ, Verkhratsky A, and Piggins H (2006) VIP receptors control excitability of suprachiasmatic nuclei neurons. Pflugers Arch 452:7-15.

Press WH, Teukolsky SA, Vetterling WT, and Flannery BP (1992) *Numerical Recipes in C.* New York: Cambridge University Press.

Quintero JE, Kuhlman SJ, and McMahon DF (2003) The biological clock nucleus: A multiphasic oscillator network regulated by light. J Neurosci 23:8070-8076.

Rohling J, Meijer JH, Vanderleest HT, and Admiraal J (2006a) Phase differences between SCN neurons and their role in photoperiodic encoding; a simulation of ensemble patterns using single unit electrical activity patterns. J Physiol Paris 100:261-270.

Rohling J, Wolters L, and Meijer JH (2006b) Simulation of day-length encoding in the SCN: From single-cell to tissue-level organization. J Biol Rhythms 21:301-313.

Sim CK and Forger DB (2007) Modeling the electrophysiology of suprachiasmatic nucleus neurons. J Biol Rhythms 22:445-453.

Strogatz SH (2000) From Kuramoto to Crawford: Exploring the onset of synchronization in populations of coupled oscillators. Physica D 143:1-20.

Terman D, Ahn S, Wang X, and Just W (2008) Reducing neuronal networks to discrete dynamics. Physica D 237:324-338.

Tiesinga PHE and Jose JV (2000) Synchronous clusters in a noisy inhibitory neural network. Journal of Computational Neuroscience 9:49-65.

Traub RD, Whittington MA, Colling SB, Buzsaki G, and Jeffreys JGR (1996) Analysis of gamma rhythms in the rat hippocampus in vitro and in vivo. J Physiol 493: 471-484.

To TL, Henson MA, Herzog ED, and Doyle FJ (2007) A molecular model for intercellular synchronization in the mammalian circadian clock. Biophys J 92:3792-3803.

Welsh DK, Logothetis DE, Meister M, and Reppert SM (1995) Individual neurons dissociated from rat suprachiasmatic nucleus express independently phased circadian firing rhythms. Neuron 14:697-706.